Available online at BCREC website: https://bcrec.id

Bulletin of Chemical Reaction Engineering & Catalysis, 15 (1) 2020, 155-174

Research Article

Structural, Thermal, Morphological, Adsorption, and Catalytic Properties of Poly(BPDAH-co-ODA/PPDA)-Ag/V_2O_5 Nanocomposites

Govindharajan Sribala[1], Balakrishnan Meenarathi[1], Ramasamy Anbarasan[2,*]

[1]Department of Polymer Technology, Kamaraj College of Engineering and Technology, Madurai-, Tamilnadu, India.
[2]Department of Chemical Engineering, National Taiwan University, Taipei-10617, Taiwan.

Received: 14th August 2019; Revised: 24th November 2019; Accepted: 26th November 2019; Available online: 28th February 2020; Published regularly: April 2020

Abstract

Thermally stable polyimides (PIs) were prepared by condensation technique at 160 °C for 5 hours in N-methylpyrrolidone (NMP) medium under N_2 atmosphere both in the presence and absence of metal (Ag) and metaloxide (MO) (V_2O_5) nanoparticles (NPs). The synthesized polymers are characterized by Fourier Transform Infra Red (FT-IR) spectroscopy, ^{1}H Nuclear Magnetic Resonance (^{1}H NMR) spectroscopy, Differential Scanning Calorimetry (DSC), Thermal Gravimetric Analysis (TGA), Scanning Electron Microscopy (SEM), Transmission Electron Microscopy (TEM), Field Emission Scanning Electron Microscopy with Energy Dispersive X-Ray (FE-SEM and EDX). The FT-IR spectrum showed a peak at 1786 cm^{-1} corresponding to the C=O stretching of dianhydride. The aromatic proton signals appeared between 6.7 and 7.5 ppm in the ^{1}H-NMR spectrum of the resultant PIs. The oxydianiline (ODA) based PI with Ag NP loaded system exhibited the highest T_g value. The apparent rate constant values for the adsorption and catalytic reduction of p-nitrophenol (PNP), Cr^{6+} and rhodamine 6G (R6G) dye were determined with the help of UV-visible spectrophotometer. Among the catalysts, the system loaded with V_2O_5 NP has higher k_{app} values. The experimental results are critically analyzed and compared with the previously available literature values.

Keywords: Polyimides; Synthesis; Characterization; DSC; FESEM; k_{app}

How to Cite: Sribala, G., Meenarathi, B., Anbarasan, R. (2020). Structural, Thermal, Morphological, Adsorption and Catalytic Properties of Poly(BPDAH-co-ODA/PPDA)-Ag/V_2O_5 Nanocomposites. *Bulletin of Chemical Reaction Engineering & Catalysis*, 15(1), 155-174 (doi:10.9767/bcrec.15.1.5595.155-174)

Permalink/DOI: https://doi.org/10.9767/bcrec.15.1.5595.155-174

1. Introduction

Polyimides (PIs) are a class of polymers which are familiar for their thermal stability, processability and mechanical properties. It has a wide domestic application. Recently, various methodologies are developed for their synthesis. By using novel techniques a number of PIs are synthesized and their structure-property relationship has been analyzed. It was found that a good number of PIs with different chemical structure had been commercialized to meet out the daily requirement of human beings. Such a thermally stable candidate can be generally prepared by condensation reaction in an economic route (*i.e.*) the reaction between dianhydride and diamine. Industrially important dianhydrides are pyromellitic dianhydride, benzophenone tetracarboxylic dianhydride and oxyphthalic dianhydride. In polymer industries,

* Corresponding Author.
Email: anbu_may3@yahoo.co.in (R. Anbarasan)

various dianhydrides are used for the preparation of PIs including benzhydrol tetracarboxylic dianyhdride [1], biphenyl tetracarboxylic dianhydride [2,3], oxydiphthalic dianhydride [4], benzophenone tetracarboxylic dianhydride [5-7], hexafluoropropane dianhydride [8,9], and pyromellitic dianhydride [10-13]. The literature report explains that the selection of dianhydride for the preparation of PIs depends on the nature of applications. It is also important that the cost of the monomer should be cheaper and free from toxicity and hazardousness. Hence, in the present work benzophenone tetracarboxylic dianhydride monomer was chosen.

For the preparation of PI, the co-monomer is considered as a diamine. Generally, ODA and PPDA are considered. The ODA based PI produced a flexible PI whereas the PPDA based PI produced a rigid PI. Their thermal and mechanical properties depend on the M_w of the PI and the method adopted for its synthesis. Various diamines including phenyl derivative of ODA [14], ODA [15-24], aniline-formaldehyde resin [25], and PPDA [26,27] have been used in the polymer industry. In order to catalyse the yield and their physical, chemical, optical and mechanical properties of the nanosized materials are added as filler. By keeping this idea in mind, the present work was designed. This work concentrates on the synthesis and characterization of two different PIs and their nanocomposites. Two different nanomaterials such as metal NP (Ag NP) and metal oxide NP (V_2O_5 NP) are added and their influence on the thermal, morphological and catalytic properties of PIs are tested and compared critically.

Due to heavy industrialization, particularly the effluents from dye industries, tannery and pharmaceutical industries, and the quality of water body are highly disturbed. The better way to solve this problem is to treat the effluents either by simple adsorption or by chemical reaction before their disposal into open environment. Among the chemical treatment, reduction is the simplest way and economically cheaper one to reduce the toxicity. The simple example is reduction of Cr^{6+} by a reducing agent into Cr^{3+} [28,29]. For an effective effluent treatment process, a supporting material, particularly heterogeneous polymer based material is required for a number of recycling process in order to avoid the leaching of the catalyst into the reaction medium. In 2017, a review article was published related to the water purification by polymer nanocomposites [30]. Chitosan supported heterogeneous catalyst was used for the reduction of PNP [31]. Poly(NIPAAm-co-AAA)/CuO nanocomposite system was utilized for the reduction of PNP [32]. A dendrimer encapsulated bimetallic nanocomposite system was utilized for the reduction of PNP [33]. Cellulose fibre supported Au NP was utilized for the reduction of organic dyes [34]. Chitosan supported TiO_2 NP was used for the reduction of organic pollutants [34]. Mei and co-workers [35] reported the PANI supported Au NP for the degradation of organic dyes. On going through the literature, it was found that few reports are available on the PI supported catalyst for the reduction of organic pollutants like PNP, R6G and inorganic pollutant like Cr^{6+}. By keeping this in inner mind, the present investigation was made, i.e. PI supported Ag and V_2O_5 nanocomposite system as a catalyst for the reduction reaction.

2. Materials and Methods

2.1 Materials

All the chemicals used are in Hipure form. N-methyl pyrrolidone (NMP), oxydianiline (ODA), sodiumborohydride ($NaBH_4$) and benzophenone-3,3',4,4'-tetracarboxylic dianhydride (BPTCDAH) were purchased from Sigma Aldrich, (India). Silver nitrate ($AgNO_3$) was purchased form *s.d.* Fine Chemicals, (India) and Vanadium pentoxide (V_2O_5) was purchased from CDH chemicals (India). Potassium dichromate, (Cr^{6+}), rhodamine6G (R6G), citric acid (CA) and p-nitrophenol (PNP) were purchased from Ranbaxy chemicals (India). Double distilled water (DDW) was used for washing purpose.

2.2 Synthesis of Ag and V_2O_5 NPs

The NPs were synthesized by a simple chemical reduction method in the presence of capping agent like citric acid. For this purpose, 1.0 g $AgNO_3$, 0.5 g of citric acid and 1.0 g of $NaBH_4$ were mixed in 100 mL DDW under mild stirring condition at room temperature for 2 hours with N_2 purging. The contents were filtered and dried in a hot air oven at 110 ºC for 6 hours. The dried product was stored in a zipper lock cover under N_2 atmosphere. The same procedure was followed for the preparation of V_2O_5 NPs.

2.3 Synthesis of PI and Its Nanocomposites

For the preparation of PI a standard literature procedure was followed with slight modification [22]. 1.0 g of PTCDAH and PPDA were taken in a 100 mL round bottomed flask (RBF).

25 mL NMP solvent was added and heated to 160 ºC for 5 hours under N_2 atmosphere with mild stirring. The polymer was precipitated by the addition of excess amount of acetone (Scheme 1). The impurities and the unreacted reactants were removed by washing the product with 100 mL of acetone. The products were dried under fume hood for overnight, weighed and stored. The yield was calculated as 91%. For the preparation of PI nanocomposites, a similar procedure was followed in the presence of 10 mg of Ag or V_2O_5 NP (Scheme 1). The % yield of PI/Ag and PI/V_2O_5 nanocomposites were determined as 93 and 97%, respectively. The weight ratio between PI and Ag or V_2O_5 NPs was maintained as 1:0.01. The higher % weight loading of NP increases the viscosity of the medium and reduces the M_w of the resultant polymer. Similar experimental procedure was followed for the preparation of ODA based PIs (Scheme 1).

2.4 Characterization

Fourier transform infrared (FTIR) spectra for the samples were recorded with the help of a Shimadzu 8400 S, Japan instrument by the KBr pelletization method from 400 to 4000 cm^{-1}. The FTIR disc was prepared under 7 tons of pressure. The surface morphology with simultaneous EDX of the polymer samples were determined by FE-SEM method using Hitachi S4800 Japan model instrument. The DSC and TGA were done using Universal V4.4A TA Instruments under nitrogen atmosphere at the heating rate of 10 ºC.min^{-1} from room temperature to 800 ºC for DSC measurements (for TGA air atmosphere was maintained). The second heating scan of the sample was considered to delete the previous thermal history of the sample. The ^{1}H-NMR (500 MHz) spectra were recorded using Varian, Unity Inova-500 NMR instrument at room temperature in deuterated DMSO solvent. The surface morphology of the samples was scanned by SEM (JSM 6300, JEOL, USA model) instrument. Transmission electron microscope (TEM) was measured using JEM-200 CX, USA. The UV-visible spectra were recorded with the help of Shimadzu 3600 NIR spectrophotometer (Japan) instrument. 2 mg of sample was dissolved in 5 mL of THF solvent from which 2 mL solution was pipetted out into a 5 mL capacity quartz cuvette and used for spectral measurement.

2.5 Catalytic Reduction Study

The primary application of this work is the utilization of polymer as a catalyst for the reduction of waste water containing different pollutants such as PNP, Cr^{6+}, and R6G. For instance, the concentration of PNP was maintained as 1×10^{-5} M solution inside the cuvette at room temperature. Then 0.10 g of polymer catalyst system (S1 or S2 or S3 or S4 or S5 or S6, Table 1) was added with mild shaking of the cuvette reactor. 15 mg of $NaBH_4$ was added as a reducing agent to the cuvette reactor with mild shaking. The UV-visible spectrum was recorded at the interval of one minute time. While increasing the reaction time, the absorbance reduced slowly at 400 nm. In the case of polymer supported catalyst system, the decrease in absorbance value is mainly due to

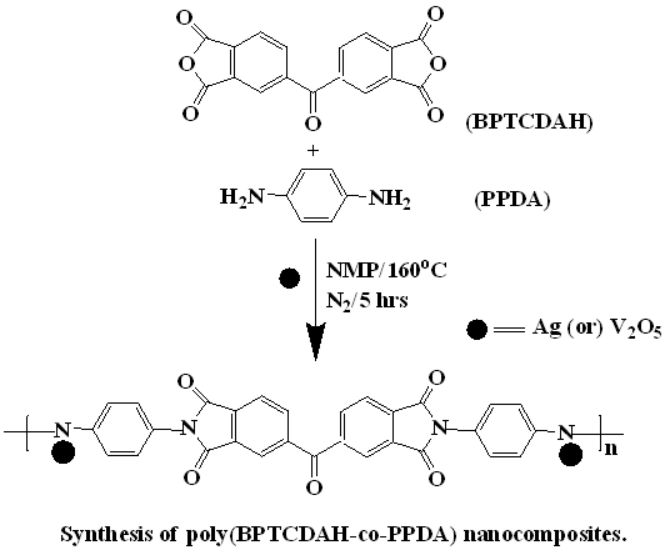

Synthesis of poly(BPTCDAH-co-PPDA) nanocomposites.

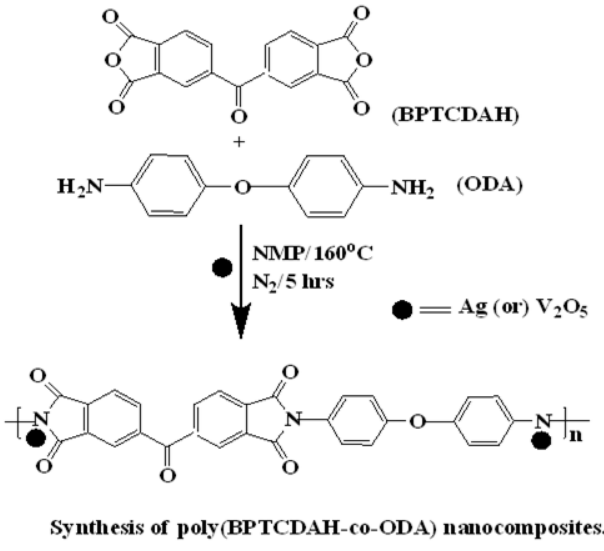

Synthesis of poly(BPTCDAH-co-ODA) nanocomposites.

Scheme 1. Synthesis of PI nanocomposites

two factors, i.e. adsorption and real catalytic reduction of PNP. From the absorbance value, the apparent rate constant (k_{app}) is determined from the slope value by drawing a plot of log (A/A_o) vs time, where A_o is an initial concentration and A is concentration at a given time. A similar procedure was followed for other systems like Cr^{6+} and R6G.

Decrease in absorbance at 400 nm due to:

PNP in the presence of catalyst system

$$= A + B + C \quad (1)$$

where A is adsorption by PI, B is surface catalytic effect of Ag or V_2O_5, and C is concentration of $NaBH_4$. The adsorption occurred through the hydrogen bonding mechanism.

Decrease in absorbance at 400 nm due to:

PNP in the absence of catalyst system

$$= A + C + D \quad (2)$$

where D is macromolecular surface catalytic effect. Here also hydrogen bonding mechanism is operated. Catalytic reduction of PNP follows the pseudo first order kinetics.

Decrease in absorbance at 375 nm due to:

Cr^{6+} in the absence of catalyst system

$$= A + C \quad (3)$$

From these the k_{app}.[Total] (E) can be calculated as follows:

$$E = F + G \quad (4)$$

where F is k_{app}.[Adsorption], and G is k_{app} (catalytic reduction).

Then, G can be calculated as follows:

$$G = E - F \quad (5)$$

The k_{app} (adsorption) depends on the nature, structure and charge on both the adsorbent and adsorbate. The absorbance can be influenced by the PI and temperature of the reaction medium. Equation (5) is applicable for all the S1 to S6 systems particularly for Ag and V_2O_5 loaded systems. In the case of S1 and S4 systems, instead of reduction, adsorption is influenced by PI and the temperature of the reaction medium.

2.6 Adsorption Study

Adsorption study was carried out in a cuvette reactor. Amount of 3 mL of water sample with PNP or Cr^{6+} or R6G was taken in a 5 mL capacity cuvette reactor. Amount of 0.10 g of PI was added with mild shaking. For every one minute time, the UV-visible spectrum was recorded and the change in absorbance was noted. Generally, it was found that while increasing the reaction time, the absorbance decreased slowly. The apparent rate constant (k_{app}) for adsorption was calculated from the slope of the

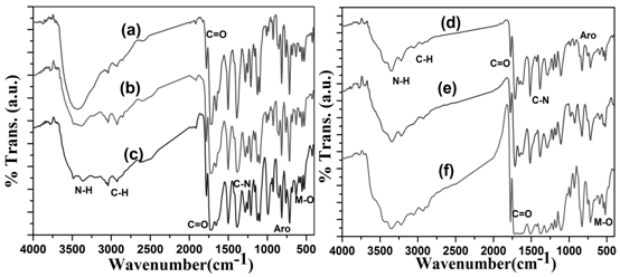

Figure 1. FT-IR spectrum of (a) S1, (b) S2, (c) S3, (d) S4, (e) S5, and (f) S6 systems.

Table 1. DSC and TGA data.

System	Code	T_g (°C)	T_d (°C)	%weight residue remained above 800 °C
Poly(BPTCDAH-co-ODA)	S1	262	513	20
Poly(BPTCDAH-co-ODA)/Ag	S2	268	525	38
Poly(BPTCDAH-co-ODA)/V_2O_5	S3	263	485	09
Poly(BPTCDAH-co-PPDA)	S4	230	482	21
Poly(BPTCDAH-co-PPDA)/Ag	S5	232	512	57
Poly(BPTCDAH-co-PPDA)/V_2O_5	S6	237	422	04

Temperature = 160 °C, time = 5 h, NMP = 25 mL, N_2 atmosphere

plot of log (A/A_o) vs time. For different PIs and pollutants systems, the UV-visible spectrum was recorded at the interval of one minute. The apparent rate constant (k_{app}) for adsorption can be determined from the slope value by drawing a plot of log (A/A_o) vs time, where A_o is an initial concentration and A is concentration at a given time.

3. Results and Discussion

3.1 Polymer Characterizations

3.1.1 FTIR spectral study

The PI synthesized with two different diamines namely ODA and PPDA is characterized here. The ODA based PI is characterized first followed by the PPDA based PI. The FT-IR spectrum of S1 system is given in Figure 1a. The N-H stretch (3416 cm^{-1}), C-H symmetric and anti-symmetric stretch (2925 and 3050 cm^{-1}, respectively) of ODA were noted. A peak at 1725 cm^{-1} is corresponding to the carbonyl stretch of dianhydride. The free dianhydride carbonyl stretching was observed at 1786 cm^{-1}. There are two different carbonyl stretching. One carbonyl stretching is involved in the PI formation whereas the other one is available at the PI chain end. This is in accordance with Ali *et al.* [35]. The aromatic bending vibrations (721 and 827 cm^{-1}) of PI were noted. Figure 1b indicates the FT-IR spectrum of S2 system. Here also one can see the above said peaks corresponding to the PI backbone. The Ag NP stretch was observed at 537 cm^{-1}. The FT-IR spectrum of S3 system is represented in Fig. 1c with the V_2O_5 stretching at 628 cm^{-1} and the stretching corresponding to the PI backbone [37]. Figure 1d indicates the FT-IR spectrum of the S4 system, i.e. the PPDA based PI. The C-H symmetric and anti-symmetric stretching of PPDA was noted at 2925 and 3048 cm^{-1} respectively. Peaks at 3221 and 3355 cm^{-1} are corresponding to the free NH_2 stretching of PPDA. This indicates that the primary amino group is attached at the polymer chain end. Peaks at 1776 and 1716 cm^{-1} are ascribed to the C=O stretching and free anhydride stretching (*i.e.*) the benzophenone moiety attached at the other end of the polymer chain. The C-N stretching (1386 cm^{-1}) and the aromatic bending vibrations (721 and 836 cm^{-1}) were also noted. Figure 1e indicates the FTIR spectrum of S5 system. Here also the above said peaks were noted. A peak at 526 cm^{-1} confirmed the presence of Ag NP. Figure 1f denotes the FT-IR spectrum of S6 system. All the peaks corresponding to PI appeared with a new peak around 1653

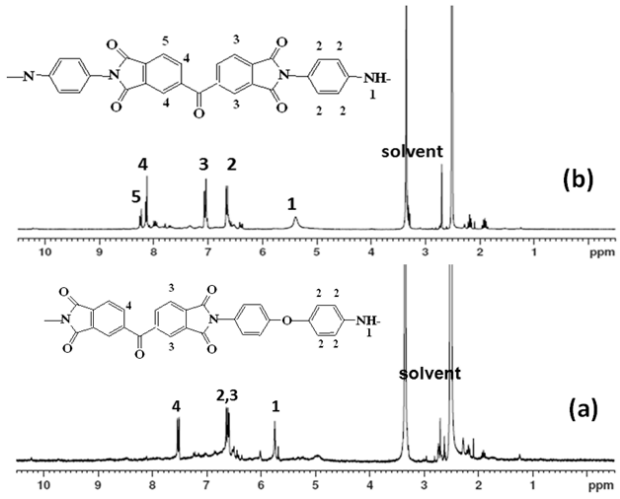

Figure 2. ^{1}H-NMR spectrum of (a) S1 and (b) S4 systems.

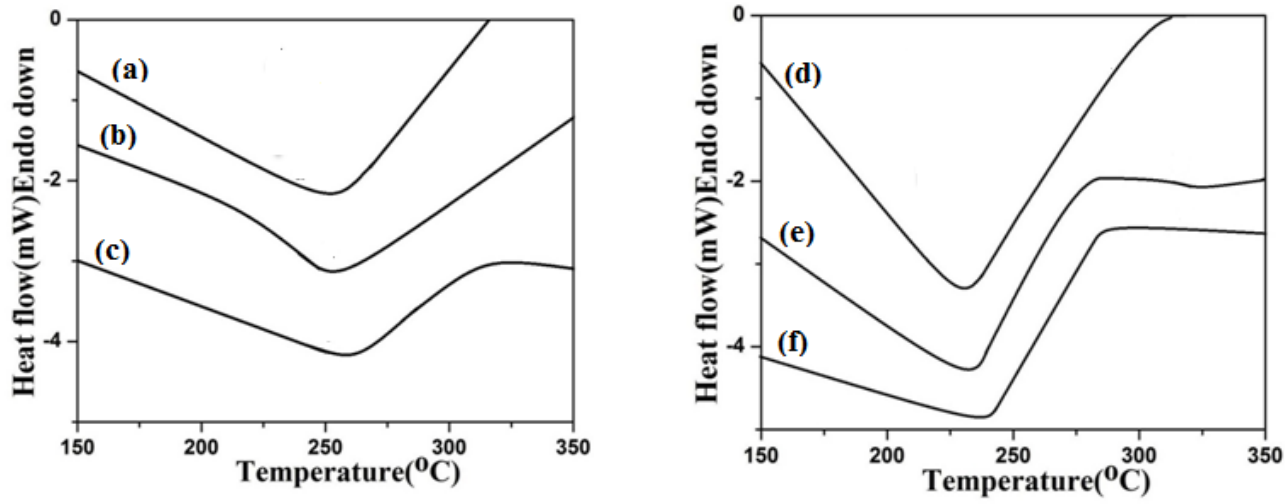

Figure 3. DSC thermogram of (a) S1, (b) S2, (c) S3, (d) S4, (e) S5, and (f) S6 systems.

cm^{-1}. This confirmed the presence of free anhydride moiety. The V_2O_5 stretching can be seen at 515 cm^{-1} [37].

3.1.2 ^{1}H-NMR study

The ^{1}H-NMR spectrum of S1 and S4 systems are studied here since they are considered as a parent PI whereas the remaining systems are Ag and V_2O_5 dispersed PI based nanocomposite systems. The N-H proton signal (5.8 ppm) of ODA confirmed the chemical structure of S1 system [2]. Meanwhile, the DMSO peaks appeared around 2-4 ppm. The ^{1}H-NMR spectrum of S4 system is given in Figure 2b. The DMSO peaks (appeared at 2.5 and 3.4 ppm) and the N-H protons of PPDA (5.3 ppm) appeared with an appearance of four new peaks at 6.7, 7.0, 8.1 and 8.3 ppm corresponding to the aromatic protons of PPDA present in the S4 backbone [6].

3.1.3 DSC study

Figure 3a shows the DSC thermogram of S1 system, which exhibits an endothermic peak at 262 °C (Table 1). Marek *et al.* [6] reported the T_g of PI which varied between 212 and 248 °C. When compared with the literature [6], the present system yielded a good result means the present nanocomposite system has higher T_g value. This can be explained as follows: i) the increase in Mw of PI; ii) chemical structure of the DAH and diamine used for the synthesis of PI; iii) existence of inter and intra molecular hydrogen bonding. The DSC thermogram of S2 system is given in Figure 3b with an endothermic peak at 252 °C. This shows the depression in T_g of the PI after the nanocomposite formation with Ag NP. Figure 3c represents the DSC trace of S3 system with an endothermic peak at 263 °C corresponding to the T_g of S3 system with increased slightly in T_g. The DSC thermogram of S4 system is given in Figure 3d. The thermogram shows an endothermic peak at 230 °C corresponding to the T_g of S4 system. The T_g of S5 system is determined from Figure 3e as 232 °C. When compared to the S4 system, the present system exhibited a slight increase in T_g. It means the added Ag NP has slight influence on the T_g. Figure 3f represents the DSC thermogram of S6 system with the T_g value of 237 °C. This confirmed that the added V_2O_5 NP slightly increased the T_g of S6 system. Table 1 summarises the T_g value of all the systems. On comparison, the S6 system exhibited the highest T_g value while considering the PPDA as a co-monomer. In over all comparison, the ODA containing PI with Ag NP exhibited the highest T_g value due to the chemical structure of the co -monomer.

3.1.4 TGA study

The TGA thermogram of S1 system is given in Figure 4a with a single step degradation process. A major weight loss peak was noted at 513 °C (Table 1) and it explained the backbone degradation of S1 system [2]. When compared with biphenyl tetracarboxylic dianhydride [2], the BPTCDAH yielded excellent T_d. Above 800 °C, the system showed 20% weight residue remained. Figure 4b denotes the TGA of thermogram of S2 system with a single step degradation process. Here the initial degradation temperature was increased. A major weight loss occurred around 525 °C with the % weight residue remained above 800 °C is 38%. The thermal stability of S3 system is given in Figure 4c.

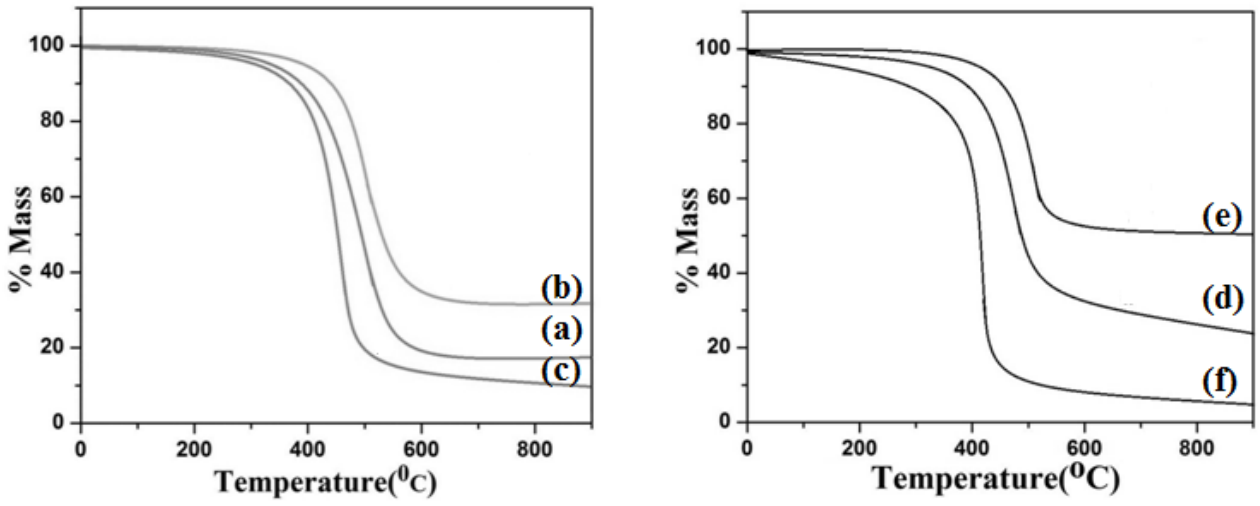

Figure 4. TGA thermogram of (a) S1, (b) S2, (c) S3, (d) S4, (e) S5, and (f) S6 systems.

The PI backbone degradation occurred at 487 ° C. Above 800 °C the system showed 9% weight residue remained. During the course of the polymerization reaction, the V_2O_5 NP increased the viscosity of reaction medium and the resultant had low molecular weight. The TGA thermogram of S4 system (Figure 4d) exhibits a single step degradation process [38] with the major weight loss at 482 °C. It can be explained on the basis of degradation of BPTCDAH. Above 800 °C the system showed 21% weight residue remained. The TGA thermogram of S5 system is shown in Figure 4e with a single step degradation occurred at 512 °C (Table 1). The important point to be noted here is the increase of initial degradation temperature in the presence of Ag NP. Above 800 °C around 57% weight residue remained. The % weight residue remained confirmed the increase in the thermal stability of S5 system. The TGA thermogram of S6 (Figure 4f) exhibits two step degradation processes. The minor weight loss appeared below 300 °C can be explained on the basis of removal of moisture and unreacted monomers or solvent. The major weight loss appeared around 422 °C is due to the degradation of PI backbone. Above 800 °C, the system exhibits <5% weight residue remained. When compared to the previous PPDA co-monomer based systems, the present system exhibited the lowest thermal stability. This can be explained as follows. It is well known that nanosized V_2O_5 is a good oxidant and at higher temperature the aerial oxidation accelerated with the help of nanosized V_2O_5. In this particular system, the nanosized V_2O_5 acts typically as an oxidative degradation catalyst. In comparison, the Ag doped PIs exhibited higher T_d and % weight residue remained above 800 °C, particularly for S2 and S5 systems. This confirmed the existence of better interaction between PI chains and Ag nanoparticles. The % weight residue remained above 800 °C for all the systems are given in Table 1.

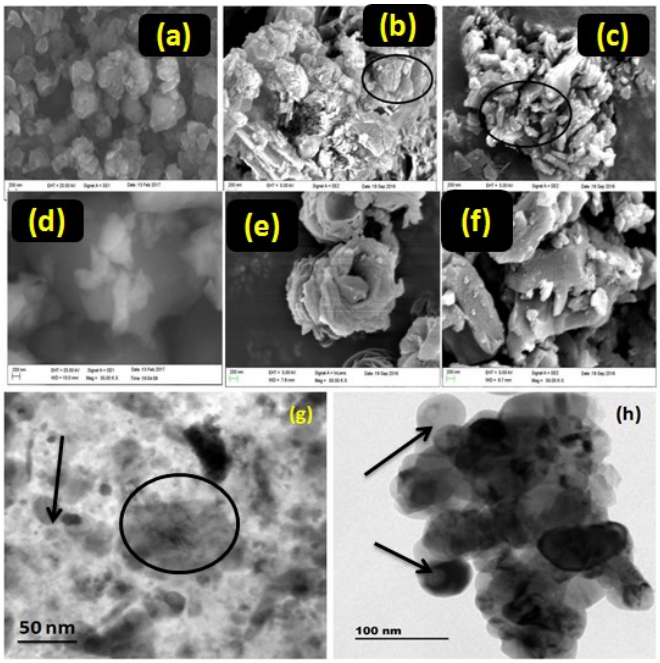

Figure 5. SEM image of (a) S1 and (d) S4 systems and FE-SEM images of (b) S2, (c) S3, (e) S5 and (f) S6 systems. TEM image of (g) Ag NP and (h)V_2O_5 NP.

3.1.5 SEM analysis

The SEM image of S1 system is given in Figure 5a with more number of agglomerated polymer NPs which can be explained that the synthesis of polymer by a commercial methodology produces polymer itself in nanosize (Table 2). Figure 5b confirms the FE-SEM image of system S2 with nanorod like morphology with the uniform distribution of Ag NP. The size was calculated as 90 nm which is indicated by the circled area. The FE-SEM image of S3 system (Figure 5c) one can see the nanorod like morphology (black circled) (Table 2) with the distribution of V_2O_5 NP. The SEM image of S4 system (Figure 5d) exhibited an irregular shaped polymer NP. The minimum length was determined as 1 μm with 250 nm breadth. This confirmed the one dimensional nanosize nature of P4 system. Arbash *et al.* [39] reported a gel like morphology for PMDAH based PI. But in the present investigation an entirely different morphology is seen. The FE-SEM image of S5 system (Figure 5e) showed a rose flower like morphology with an agglomeration of Ag NPs. The minimum size of Ag NP was determined as 50 nm. The system exhibited nanorod like morphology (Table 2). The length of the rod was calculated as >1 μm and with the breadth of 100 nm. The FE-SEM image of S6 system is

Table 2. Morphology and % elements data.

System	Shape	% Elements				
		C	N	O	Ag	V
S1	Irregular	-	-	-	-	-
S2	Rod	46	16	32	11	-
S3	Rod	44	18	32	-	6
S4	Irregular	-	-	-	-	-
S5	Rod	46	15	32	6.8	-
S6	Irregular	48	17	35	-	3.1

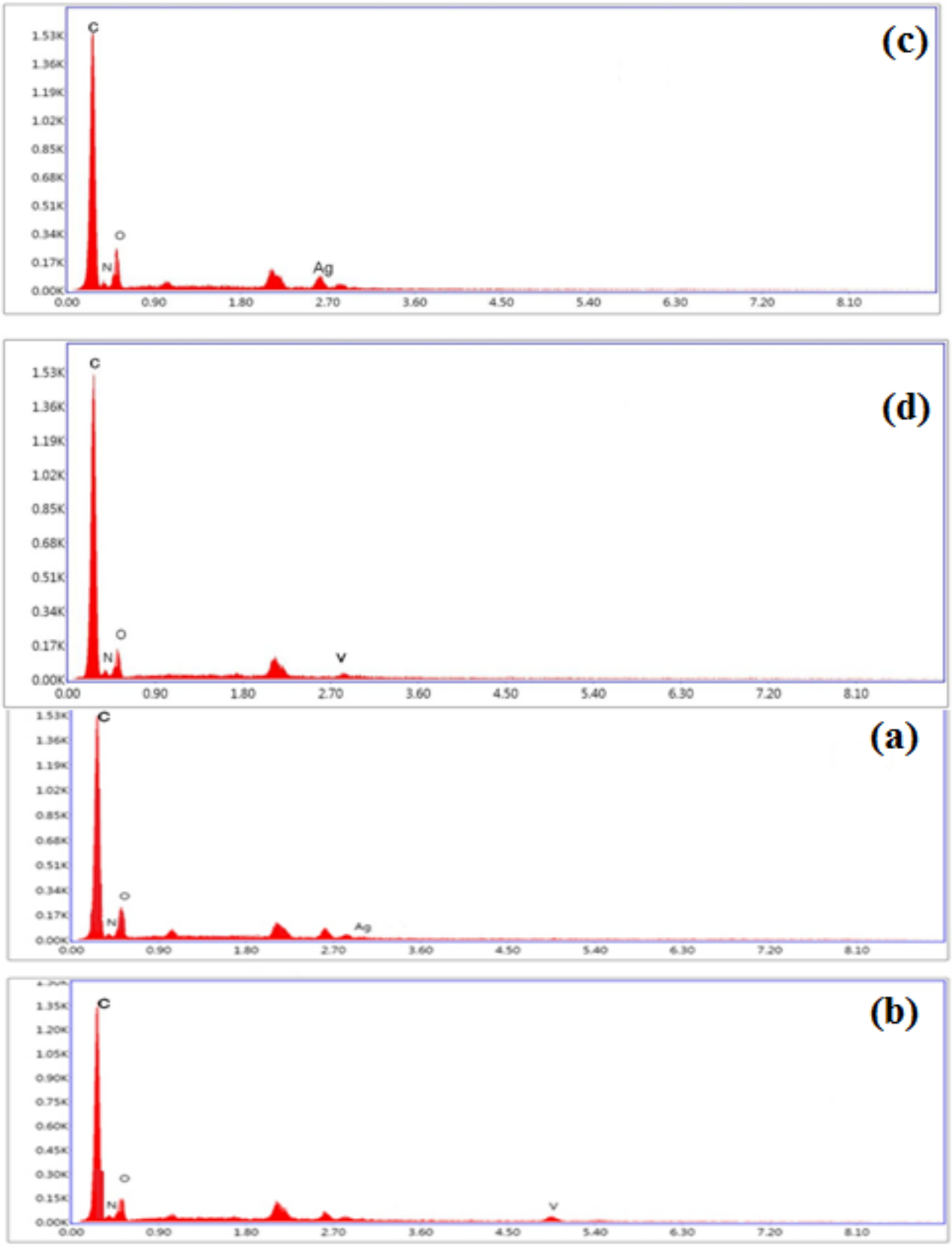

Figure 6. EDX spectrum of (a) S2, (b) S3, (c) S5 and (d) S6 systems.

given in Figure 5f. The morphology was like a broken stone with an irregular shape and size, nanosized spherical particles with the size of 80 nm. This is due to the V_2O_5 NP. Here nanofibre morphology was not observed. This indicates that the polymer after the nanocomposite formation with V_2O_5 NPs, the fibrous morphology was with an irregular shape (Table 2) and size. This declared that each NP has its own influence on the surface morphology of the polymer (*i.e.*) the morphology of the polymer can be altered. Jwo *et al.* [40] reported different morphology for PI in the presence of silica and this report supported the above said statement. Thus the SEM image concluded the size, shape and morphology of the PI and its nanocomposite systems. For the sake of comparison, the TEM image of Ag (Figure 5g) and V_2O_5 NPs (Figure 5h) are given here. The size of Ag NP was found to be 15-25 nm with some agglomerated NPs. The size of V_2O_5 NP was found to be 65-85 nm with distorted spherical morphology with more agglomeration.

3.1.6 EDX report

In the EDX spectrum of S2 system (Figure 6a), the % content of C, N, O and Ag was determined as 46, 16, 27, and 11 %, respectively and shown in Table 2. The appearance of Ag confirmed the presence of Ag NPs in the P2 system. Figure 6b represents the EDX spectrum of S3 system. The % content of C was found to be 44%. The % content of N and O was determined as 18 and 32%, respectively. In this system 6% of V was found and its appearance confirmed the formation of Vanadium nanocomposite system. In the EDX spectrum of S5 system (Figure 6c), the % C, N, and O was calculated as 46, 15 and 32%, respectively (Table 2). The % content of Ag NP was determined as 6.89%. This confirmed the presence of Ag NP in the S5 system. Figure 6d indicates the EDX spectrum of S6 system. In this case the % C, N, O was calculated as 45, 17 and 35%, respectively. The % of V was calculated as 3.11% (Table 2). Thus the EDX study concluded that the PI nanocomposite systems contain the Ag and V_2O_5 NPs.

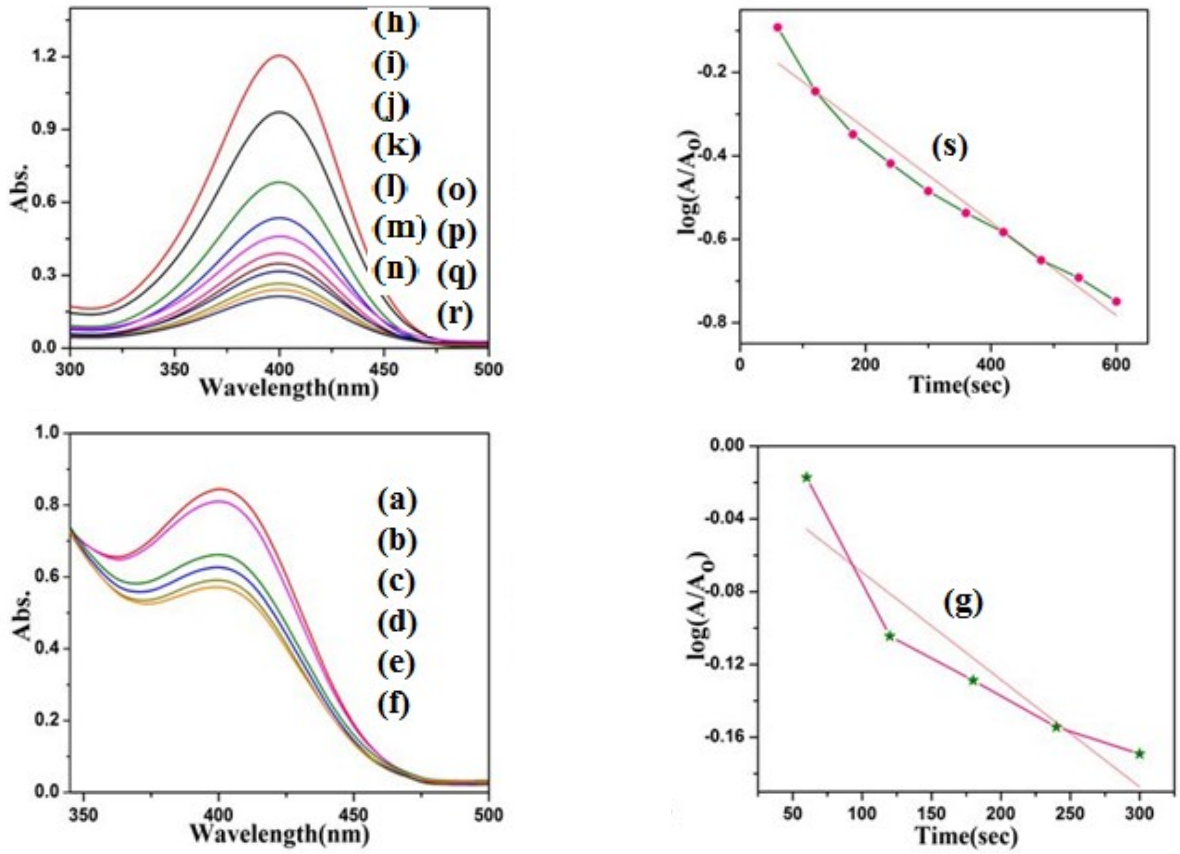

Figure 7. UV-visible spectrum of PNP (a-f) taken at the interval of one min in the presence of S1 system and plot of log (A/A_o) vs time (g). The UV-visible spectrum of PNP (h-r) taken at the interval of one min in the presence of S4 system and the plot of log (A/A_o) vs time (s).

3.2 Catalytic Reduction Study

Generally, the benzophenone based PI is used in the membrane technology. For the first time, the applications of benzophenone based PI is brought into the catalysis field. Under the given experimental conditions, the catalytic reduction of PNP was carried out. It exhibited an absorbance peak at 401 nm. The UV-visible spectrum of PNP taken at the interval of 1min time during the reduction reaction is given in Figure 7(a-f). While increasing the reduction reaction time the absorbance reduced slowly at 401 nm. Within 6 minutes 88% of PNP was reduced into aminophenol (AP). The decrease in absorbance at 401 nm is associated with two important factors namely, adsorption and real catalytic reduction or reduction reaction. In the first step, the total apparent constant (k_{app}) was determined using the UV-visible absorbance spectral data. The total k_{app} value was determined from the slope of the plot of $\log(A/A_o)$ vs time (Figure 7g) as 0.59×10^{-3} sec^{-1} (Table 3). The k_{app} value of adsorption was calculated as 0.585×10^{-3} sec^{-1} (Table 3). The remaining k_{app} value of 0.005×10^{-3} sec^{-1} is associated with two factors: (i) surface catalytic reaction and (ii) reduction by $NaBH_4$. It is well known that the S1 system does not carry any catalyst like Ag or V_2O_5 NP. In this situation, the PI system may behave like a macro surface catalyst. As a result, the PNP is reduced into AP. From the literature it was understood that the catalytic reduction of PNP follows the pseudo first order kinetics. This confirmed that the PI acted as a macro catalyst towards the reduction of PNP. The added reducing agent decreases the pH of the reaction medium and increases the adsorption. Four H^+ ions produced from $NaBH_4$ strengthened the pH of 1.5 and accelerated the adsorption process. Without the surface catalytic effect (either by metal or metal oxide NP), the PNP will not be reduced to AP. The 0.005×10^{-3} sec^{-1} k_{app} value is due to the added $NaBH_4$ and not due to the real reduction reaction in the case of PNP. Mei *et al.* [37] reported the k_{app} value for the catalytic reduction of PNP using Fe_3O_4@PANI@Au ternary polymer nanocomposite system as 8.63×10^{-3} sec^{-1}. When compared with the literature value, the present system yielded an extremely lower k_{app} value due to the absence of metal or metal oxide NP.

The macro surface catalytic effect of S4 system towards the reduction of PNP under the same experimental conditions was tested. Figure 7 (h-r) indicates the UV-visible spectrum of PNP taken at the interval of 1 min. The spectrum shows one absorbance peak at 401 nm. While increasing the reduction reaction time, the absorbance decreased slowly at 401 nm. This confirms the reduction of PNP into AP or simple adsorption by S4 system. This spectrum infers that within 13 min 85 % of PNP was converted into AP. In order to find out the total k_{app} value, the plot of log (A/A_o) vs time (Figure 7s) was drawn. It was found to be a straight line but with decreasing trend. The slope value was determined from which the total k_{app} value was calculated as 1.12×10^{-3} sec^{-1} (Table 3). For S4 system also a separate adsorption experiment was carried out. From the absorbance value, the k_{app} value for adsorption was calculated as 1.158×10^{-3} sec^{-1}. From these data, one can easily find out the k_{app} value for the reduction reaction as 0.004×10^{-3} sec^{-1} (Table 3). The reduction of the k_{app} value confirmed the poor catalytic role of macro sized S4 system. In other words under strong acidic pH, the adsorption of PNP was increased. In the absence of Ag or V_2O_5 NPs the catalytic reduction of PNP into AP is not possible. On analysis, both S1 and S4 yielded almost closer k_{app} values for ad-

Table 3. k_{app} value of different systems

System	k_{app} (10^{-3}) (sec^{-1})								
	PNP			Cr^{6+}			R6G		
	Total	Ads	Cat red	Total	Ads	Cat red	Total	Ads	Cat red
S1	0.59	0.585	0.005	2.10	1.32	0.78	0.22	0.15	0.07
S2	5.69	2.810	2.880	1.59	0.72	0.87	2.34	1.12	1.22
S3	6.31	4.150	2.160	1.22	0.68	0.54	2.79	1.28	1.51
S4	1.12	1.116	0.004	1.17	0.93	0.24	1.40	0.88	0.52
S5	2.53	1.410	1.120	2.55	1.38	1.17	3.26	1.59	1.67
S6	1.65	0.720	0.930	2.42	1.14	1.28	3.52	1.71	1.81

sorption under strong acidic pH but two times higher k_{app} value for adsorption by S4 system. This can be explained on the basis of chemical structure of the S4 system. In the case of S1 and S4 systems, the k_{app} values are very lower when compared with Mei *et al.* [37] report due to the absence of nano catalyst for the reduction of PNP.

The study on influence of Ag NP on the catalytic reduction reaction of PNP was carried out. The UV-visible spectrum of PNP recorded in the presence of S2 system at the interval of one minute is given in Figure A1(a-h). While increasing the reaction time the absorbance at 400 nm decreased gradually. This confirmed the catalytic reduction of PNP into AP. It was very interesting to note that within 7 min 84% of PNP was reduced into AP. The total k_{app} value was determined by drawing the plot of log (A/A_o) vs time (Figure A1 i). The total k_{app} value was calculated as 5.69×10^{-3} sec^{-1} (Table 3). As per the procedure, a separate experiment was carried out to find out adsorption from which the k_{app} value was calculated as 2.81×10^{-3} sec^{-1}. From this value, it is easy to calculate the k_{app} value for the real catalytic reduction reaction as 2.88×10^{-3} sec^{-1}. In the present system, it was found that the catalytic reduction reaction and the adsorption are having almost equal k_{app} value. It means that these two reactions are competitive one. When compared with S1 and S4 systems, the present system yielded higher k_{app} value due to the presence of Ag NP. Islam *et al.* [35] studied the catalytic reduction of PNP in the presence of Au loaded cellulose fiber (CF). The reported k_{app} values are 6.67×10^{-5} sec^{-1} and 1.03×10^{-2} sec^{-1} for pristine CF and CF-Au-2.87 systems, respectively. When compared with their value, the present S2 system produced very lower k_{app} value. This is due to the difference in the polymer structure and the metal nano catalyst used for the PNP reduction. Still the adsorption value increased under acidic pH.

The catalytic activity of S5 system was tested towards the reduction of PNP. The UV-visible spectrum of PNP taken at one min time interval in the presence of S5 catalyst is shown in Figure A1 (j-p). Within 7 min 91% of PNP was reduced into AP. This confirmed the catalytic activity of S5 system. The total k_{app} value was determined by drawing a plot between log (A/A_o) and time (Figure A1 q). The plot showed a straight line with decreasing trend, from which the total k_{app} value was calculated as 2.53×10^{-3} (Table 2). The k_{app} value for the adsorption and real catalytic reduction reactions were calculated as 1.41×10^{-3} sec^{-1} and 1.12×10^{-3} sec^{-1}, respectively (Table 3). When compared to the S2 system, the present system exhibited lower k_{app} value for catalytic reduction reaction. This declared the catalytic activity of Ag NP. On comparison among S1, S2, S4 and S5 systems, the S4 systems yielded higher k_{app} value for the reduction of PNP. Liu *et al.* [41] reported the catalytic reduction of PNP using Au/PAN nanofibrous membrane with the k_{app} value of 4.66×10^{-4} sec^{-1}. When compared with their value, the present S4 system yielded a good k_{app} value towards the reduction of PNP.

The catalytic activity of S3 system was tested towards the reduction of PNP {Figure A2 (a-g)}. During the course of the reduction reaction the absorbance decreased at 400 nm slowly. This proved that the PNP was reduced into AP in the presence S3 system as a catalyst and $NaBH_4$ as a reducing agent. The catalytic activity of V_2O_5 NP present in the S3 system was further confirmed by plotting log (A/A_0) vs time (Figure A2 h). The plot showed a decreasing trend with the total k_{app} value of 6.31×10^{-3} sec^{-1} (Table 2). For adsorption, a separate experimental work was conducted and the k_{app} value was determined as 4.15×10^{-3} sec^{-1}. The k_{app} value for the real catalytic reduction reaction was calculated as 2.16×10^{-3} sec^{-1} (Table 3). In comparison with S2 system, the S3 system yielded somewhat lower k_{app} value. When compared with the literature value [41], the S3 system yielded somewhat good k_{app} value.

The catalytic activity of S6 system was tested towards the reduction of PNP under the same experimental conditions as mentioned above and shown in Figure A2 (i-p). Within 8 min 95 % of PNP was reduced into AP. For this system the total k_{app} value was determined from the plot of log (A/A_o) vs time (Figure A2 q). From the slope value the total k_{app} value was calculated as 1.65×10^{-3} sec^{-1} (Table 3). As usual, a separate experiment was carried out for the determination of k_{app} value for adsorption and determined the same as 0.72×10^{-3} sec^{-1}. From this, the k_{app} value for the catalytic reduction reaction was determined as 0.93×10^{-3} sec^{-1} (Table 3). In comparison with S3 system, the present system yielded very lower k_{app} value. In over all comparison, the S2 system produced an excellent k_{app} value for the catalytic reduction of PNP. The PI/V_2O_5 nanocomposite system provided a good k_{app} value than the PAN/Au nanocomposite system [41] towards the catalytic reduction of PNP.

It is well known that Cr^{6+} is more toxic than Cr^{3+}. Hence it is necessary to remove or reduce the toxicity of Cr^{6+} ion by a simple adsorption

or reduction method. The ultimate aim of the present investigation is to reduce the toxicity of Cr^{6+} in the presence of S1 system as a catalyst. Figure A3(a-i) confirmed the UV-visible spectrum of Cr^{6+} taken at different time interval in the presence of S1 system. Here also while increasing the reaction time, the absorbance at 369 nm decreased gradually. At the end of 9 min, 94% of Cr^{6+} was reduced to Cr^{3+}. The catalytic activity of S1 system can be further confirmed by drawing a plot of log (A/A_0) vs time (Figure A3j). From the slope value, the total k_{app} value was calculated as 2.1×10^{-3} sec^{-1} (Table 2). It is well known that the Cr^{6+} can be reduced into Cr^{3+} with the help of $NaBH_4$ even in the absence of a catalyst. In the presence of metal or metaloxide NP catalyst, the catalytic reduction of Cr^{6+} will be very fast. In S1 system such a catalyst is not available. Even then the absorbance at 369 nm corresponding to Cr^{6+} decreased continuously. This confirmed the catalyst free reduction of Cr^{6+}. Moreover, the Cr^{6+} normally appears at 375 nm but in the present work it appeared at 369 nm due to the decrease in pH of the medium and addition of $NaBH_4$. The hydrogen atom loses its electron to the reaction medium and becomes H^+. This further decreases the pH of the reaction medium. As a result the Cr^{6+} appeared at 369 nm (blue shifting). As explained previously, the decrease in concentration of Cr^{6+} can be explained on the basis of two factors namely, adsorption and real catalytic reduction reaction. Here reduction reaction really occurred due to the addition of $NaBH_4$ at the same time adsorption is possible through the formation of co-ordination bond between Cr^{6+} and PIs. This can be further confirmed by conducting a separate experiment for the adsorption reaction in the absence of catalyst and $NaBH_4$. Again it was found that the absorbance decreased at 375 nm continuously. The k_{app} value for adsorption and reduction reaction was determined as 1.32×10^{-3} sec^{-1} and 0.78×10^{-3} sec^{-1} (Table 3), respectively. This proved that the adsorption is a dominant process than the reduction reaction in the presence of S1 system towards Cr^{6+}. The k_{app} value for the Zn/Fe_2O_4 loaded PANI was determined

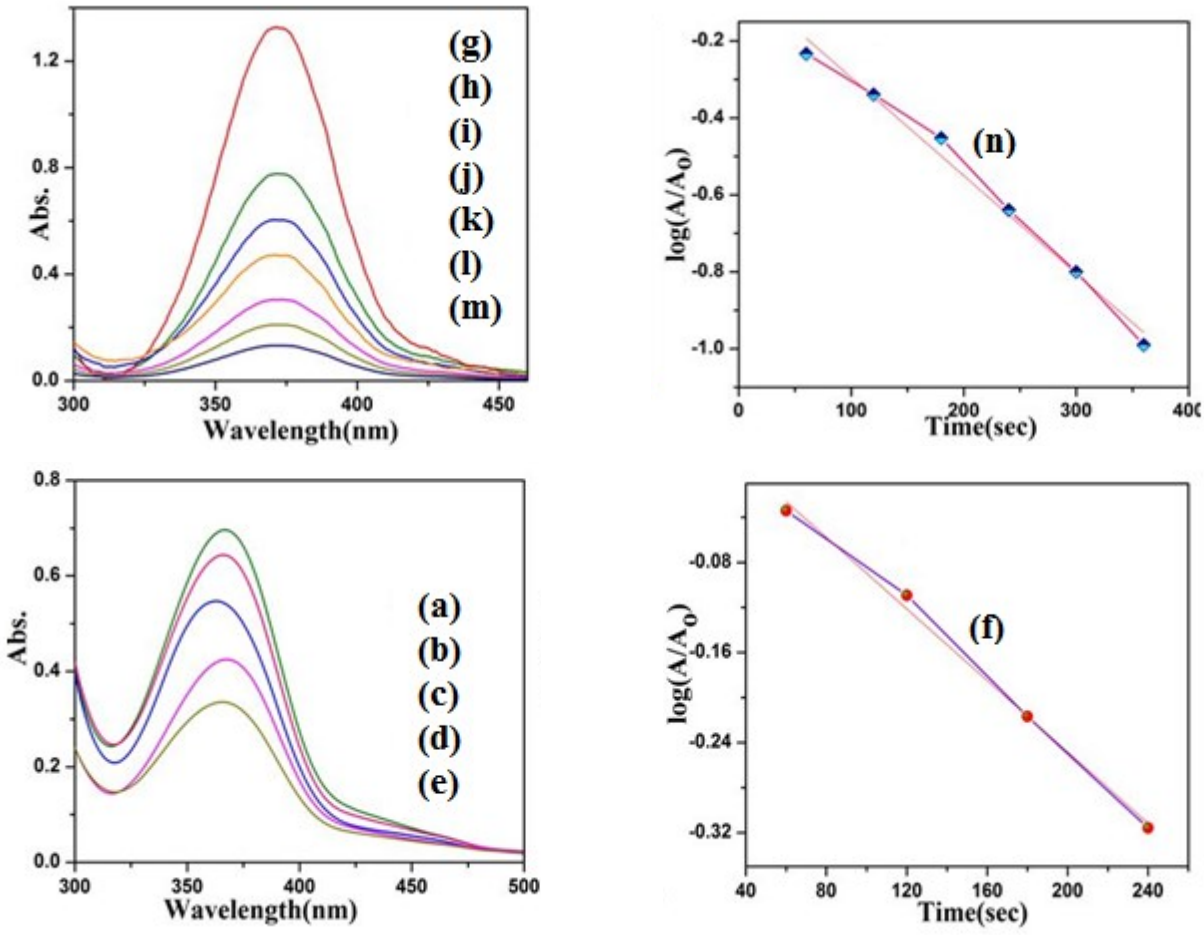

Figure 8. UV-visible spectrum of Cr^{6+} (a-e) taken at the interval of one min in the presence of S2 system and plot of log (A/A_o) vs time (f), UV-visible spectrum of Cr^{6+} (g-m) taken at interval of one min in the presence of S5 system and plot of log (A/A_o) vs time (n).

as 0.54×10^{-3} sec^{-1} towards the photocatalytic reduction of Cr^{6+} [42]. On comparison, the S1 system yielded higher k_{app} value even in the absence of metal or metaloxide nanocatalyst. Moreover, the adsorption due to PANI was not included by Patnaik *et al.* [42]. This study indicates that the Cr^{6+} can be reduced even in the absence of a metal or metaloxide nanocatalyst.

Similarly, the influence of S4 system was tested towards Cr^{6+} and shown in Figure A3 (k-u). The spectrum shows one absorbance peak at 372 nm corresponding to the Cr^{6+}. Here also while increasing the reaction time the absorbance reduced at 372 nm slowly. Within 11 min 90% of Cr^{6+} was reduced into Cr^{3+}. The k_{app} value was determined by drawing a plot of log (A/A_o) vs time (Figure A3v). The total k_{app} value was as 1.17×10^{-3} sec^{-1} (Table 2). But the decrease in concentration is due to adsorption also. Hence, it is necessary to find out the k_{app} values corresponding to the adsorption and reduction reactions separately. The values are 0.93×10^{-3} sec^{-1} and 0.24×10^{-3} sec^{-1} (Table 3) for adsorption and reduction reactions respectively. Here the process of adsorption is found to be dominant than the chemical reduction reaction. When compared with the S1 system, the present system yielded somewhat lower k_{app} values. When compared with literature [42] the present S4 system yielded lower k_{app} value due to the difference in the polymer backbone and absence of nanocatalyst.

The reduction of Cr^{6+} was done in the presence of S2 system (*i.e.*) PI loaded with Ag NP. Figure 8 (a-e) shows the reduction in absorbance at 366 nm gradually. The blue shift in the peak confirmed the role of Ag NP in the chemical reduction reaction. Within 5 min. 65% of Cr^{6+} was reduced into Cr^{3+}. The plot of log (A/A_0) vs time is shown in Figure 8(f). The plot exhibited a straight line but with decreasing trend. The total k_{app} value was calculated as 1.59×10^{-3} sec^{-1} (Table 3). Meanwhile, the k_{app} values for adsorption and catalytic reduction reaction were determined as 0.72×10^{-3} sec^{-1} and 0.87×10^{-3} sec^{-1}, respectively (Table 3). On comparison, the S2 system exhibited the highest k_{app} value for catalytic reduction and declared that the S2 system containing Ag NP has high surface area. When compared with the Zn/Fe_2O_4 loaded PANI nanocomposite system without the consideration of adsorption [42], the PI/Ag nanocomposite system produced higher k_{app} value towards the reduction of Cr^{6+} (by considering the adsorption value).

The catalytic activity of S5 system loaded with Ag NP was tested towards the reduction of Cr^{6+}. It was found that the absorbance peak at 372 nm decreased slowly with increase in time (Figure 8 g-m). Within 7 min 95% of Cr^{6+} was reduced into Cr^{3+} in the presence of S5 system. By using the usual plot of log (A/A_o) vs time (Figure 8 n), the total k_{app} value was calculated as 2.5×10^{-3} sec^{-1} (Table 3). The k_{app} values for adsorption and catalytic reduction reaction were determined as 1.38×10^{-3} sec^{-1} and 1.17×10^{-3} sec^{-1} (Table 3), respectively. When compared with S2 system, the present system yielded somewhat improved k_{app} value. Again, when compared with the literature value [42], the present system yielded higher k_{app} value towards the reduction of Cr^{6+}.

The catalytic activity of S3 system was tested under identical conditions and the UV-visible spectrum of PNP is shown in Figure A4 a-g. It was found that within 6 min 97% of Cr^{6+} was reduced in to Cr^{3+}. The total k_{app} value was determined from Figure A4 (h) as 1.22×10^{-3} sec^{-1} (Table 3). As per the procedure, the k_{app} values for the adsorption and catalytic reduction reactions were determined as 0.68×10^{-3} sec^{-1} and 0.54×10^{-3} sec^{-1}, respectively (Table 3). This proved that the catalytic reduction reaction is less favourable than the adsorption process. The photocatalytic reduction of Cr^{6+} in the presence of Zn/Fe_2O_4@PANI [42] yielded higher k_{app} value without the consideration of adsorption.

The catalytic activity of S6 system was tested towards the reduction of Cr^{6+}. It was found that the absorbance peak decreased at 372 nm slowly with increase in reaction time (Figure A4 i-n). It was found that within 6 min 91% of Cr^{6+} was reduced into Cr^{3+}. The total k_{app} value was determined by plotting log (A/A_o) vs time (Figure A4 o) as 2.42×10^{-3} sec^{-1} (Table 3). The k_{app} value for the adsorption and catalytic reduction reactions were determined as 1.14×10^{-3} sec^{-1} and 1.28×10^{-3} sec^{-1} (Table 3), respectively. When compared with S3 system, the S6 system yielded somewhat lower k_{app} value for the catalytic reduction reaction. On comparison with the literature [42], the present system yielded higher k_{app} value. On overall comparison, the S6 system exhibited the highest k_{app} value. This confirmed that the V_2O_5 NP is a suitable catalyst system for the catalytic reduction of Cr^{6+}.

Catalytic activity of S1 system was tested towards the reduction of R6G dye under the experimental conditions mentioned above. From the UV-visible spectrum (Figure A5 a-g) it was found that while increasing the reduction time, the absorbance at 525 nm decreased slowly. Within 6 min 80% of R6G dye reduced. The total k_{app} is determined by plotting log (A/A_0) vs

time (Figure A5 h) as 0.22×10^{-3} sec^{-1} (Table 3). The R6G dye molecule is reduced with the help of $NaBH_4$ in the absence of a catalyst. In order to confirm the dye adsorption by S1 system, a separate adsorption experiment was made in the absence of a reducing agent. The k_{app} value for the adsorption was calculated as 0.15×10^{-3} sec^{-1}. From this one can calculate the k_{app} for the real reduction reaction as 0.07×10^{-3} sec^{-1} (Table 3). Adsorption is the most favourable one than the reduction reaction. Saranya and co-workers [43] reported the V_2O_5 NP loaded Chitosan Schiff base for the catalytic reduction of R6G dye with the k_{app} value of 9.70×10^{-3} sec^{-1}. The present S1 system towards the reduction of R6G yielded lower k_{app} value due to the absence of nanocatalyst.

Ultimately, the catalytic application of S4 system was towards the reduction of R6G. The UV-visible spectrum of R6G is given in Figure A5 (i-r). It was found that while increasing the reaction time the absorbance at 525 nm decreased. The extended double bond of R6G was reduced chemically. At the same time adsorption of R6G by the S1 system was occurred through the hydrogen bonding mechanism. Within 10 min 92% of R6G reduced. To determine the total k_{app} value, a plot was drawn between log (A/A_o) and time (Figure A5 s). As usual the plot was found to be a straight line with decreasing trend. The total k_{app} value was determined as 1.40×10^{-3} sec^{-1} (Table 3). The k_{app} values for the adsorption and reduction of R6G was determined as 0.88×10^{-3} sec^{-1} and 0.52×10^{-3} sec^{-1} (Table 3), respectively. On comparison, the P4 system exhibited the highest k_{app} value for the reduction of R6G. When compared with Saranya *et al.* [43] report, the present system yielded lower k_{app} value towards the reduction of R6G.

The catalytic activity of S2 system was tested towards the reduction of R6G and is shown in Figure A6 (a-h). It was clearly observed that absorption decreased at 527 nm gradually.

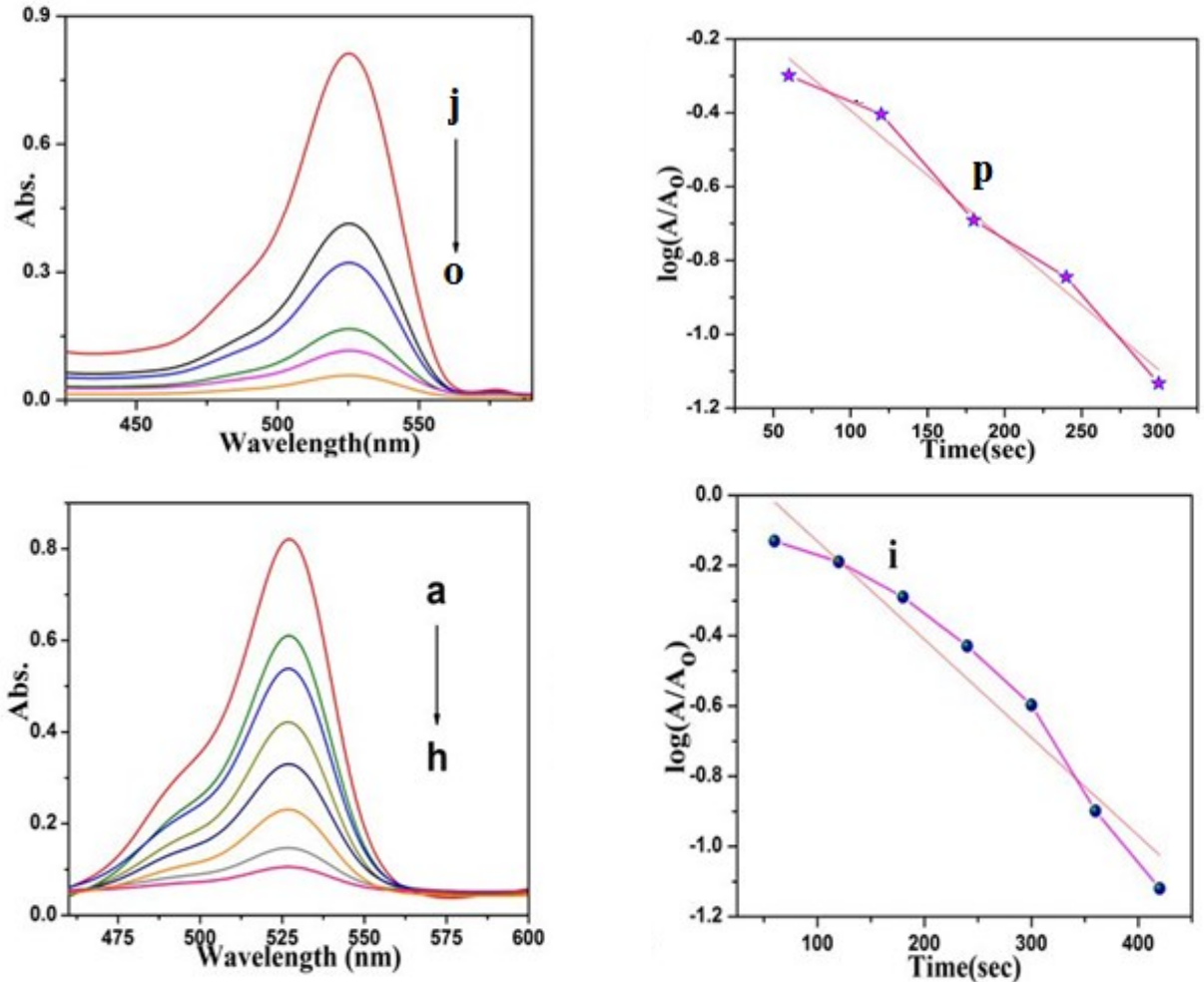

Figure 9. UV-visible spectrum of R6G (a-h) taken at the interval of one min in the presence of S3 system and the plot of log (A/A_o) vs time (i). The UV-visible spectrum of R6G (j-o) taken at the interval of one min in the presence of S6 system and plot of log (A/A_o) vs time (p).

Within 8 min 96% of R6G reduced. Further, the total k_{app} value was calculated from the plot of log (A/A_o) vs time (Figure A6 i) as 2.34×10^{-3} sec^{-1} (Table 3). The k_{app} values for adsorption and catalytic reduction reaction was determined as 1.12×10^{-3} sec^{-1} and 1.22×10^{-3} sec^{-1} (Table 3) respectively. When compared to the S1 system, the Ag nanocomposite system showed higher k_{app} value. This confirmed the catalytic nature of Ag NPs. Even in the presence of Ag NP, the k_{app} value was found to be lower than Chitosan Schiff base/V_2O_5 nanocomposite system [43].

The catalytic activity of S5 system was tested towards the reduction of R6G (Figure A6 j-o). In order to calculate the total k_{app} value, the plot of log (A/A_o) vs time (Figure A6 p) was drawn and it was found to be a straight line with decreasing trend. From the slope value, the total k_{app} value was calculated as 3.26×10^{-3} sec^{-1} (Table 3). From Table 3 it was found that the k_{app} value for the adsorption and catalytic reduction was 1.59×10^{-3} sec^{-1} and 1.67×10^{-3} sec^{-1} (Table 3) respectively. When compared to S1 system, the Ag nanocomposite system exhibited higher k_{app} value. This confirms the catalytic activity of Ag nanoparticles. The S5 system exhibited the highest k_{app} value. When compared with the literature report [43] the present system yielded lower k_{app} value.

The catalytic activity of S3 system was tested towards the reduction of R6G (Figure 9(a-h)). While increasing the reduction reaction time, the absorbance decreased at 526 nm. Within 8 min 95% of R6G reduced. The plot of log (A/A_o) vs time (Figure 9 i) was drawn and it was found to be a straight line with decreasing trend. The total k_{app} value was found to be 2.79×10^{-3} sec^{-1} (Table 3). Table 3 showed that the k_{app} values for the adsorption and catalytic reduction were 1.28×10^{-3} sec^{-1} and 1.51×10^{-3} sec^{-1}, respectively. It seems that the S3 system exhibited somewhat higher k_{app} value towards the catalytic reduction of R6G. In the presence of Chitosan Schiff base/V_2O_5 nanocomposite system [43], the k_{app} value was found to be very high when compared with the PI V_2O_5 nanocomposite system. Apart from the size of the nanocatalyst, the polymer backbone played a vital role in the reduction of R6G. In a comparative analysis, the Chitosan Schiff base has more hydrogen bond than the PI system due to the absence of –OH and $–NH_2$.

Similarly, the catalytic activity of S6 system was tested towards the reduction of R6G under similar experimental conditions. The UV-visible spectrum is shown in Figure 9(j-o). Here also the absorbance reduced at 523 nm and within 6 min 96% of R6G was reduced. The catalytic activity of S6 system is further confirmed by drawing the plot of log (A/A_o) vs time (Figure 9 p). It was found to be a straight line with negative trend. From the slope value the total k_{app} value was calculated as 3.52×10^{-3} sec^{-1} (Table 3). The k_{app} values for the adsorption and catalytic reduction reactions were determined as 1.71×10^{-3} sec^{-1} and 1.81×10^{-3} sec^{-1} (Table 3), respectively. When compared with S3 system, the present S6 system exhibited little bit improved k_{app} value. The V_2O_5 nanocomposite system exhibited the highest k_{app} value. When compared with the literature report [43], the present system yielded lower k_{app} value towards the reduction of R6G dye.

4. Conclusions

The positive points which are supporting to this work is shown here as conclusions. The FT-IR spectrum showed a carbonyl and amino stretching around 1785 and 3500 cm^{-1}, respectively and confirmed the PI formation. The aromatic protons of ODA and PPDA units appeared between 6.6 and 7.6 ppm. The V_2O_5 NPs loaded PI exhibited slight increase in T_g value. The Ag NPs loaded PI showed 30% of above 800 ºC. The Ag NPs embedded PI exhibited the nanorod like morphology. The size of V_2O_5 NP was determined as 65-85 nm with agglomeration by TEM. The EDX study concluded that 3% of V was available in the PPDA based PI system. The Poly(BPTCDAH-co-ODA)/V_2O_5 nanocomposite system exhibited the highest k_{app} value for the adsorption of PNP. The Poly(BPTCDAH-co-ODA)/Ag nanocomposite system showed the highest k_{app} value for the catalytic reduction of PNP. This proved that whether the adsorption or catalytic reduction reaction depends on the chemical structure and surface charge of the materials.

Acknowledgement

We express our sincere thanks to Dr. N. Sundararajan, Associate Professor, Department of English, KCET, Virudhunagar for his valuable help during this manuscript preparation work.

Compliance with ethical standards

Conflict of interest

Authors have no conflicts of interest to declare.

List of Abbreviations

PI : Polyimide
PMDAH : Pyromellitic dianhydride
ODA : Oxydianiline
PPDA : p-phenylenediamine
FT-IR : Fourier transform infrared
NMR : Nuclear magnetic resonance
DSC : Differential scanning calorimetry
TGA : Thermogravimetric analysis
FE-SEM : Field emission scanning electron microscope
AFM : Atomic force microscope
NP : Nanoparticle
NMP : N-methylpyrrolidone
MWCNT : Multiwalled carbon nanotube
PNP : p-Nitrophenol
R6G : Rhodamine 6G
DMF : Dimethylformamide
SMF : Standard measuring flask
SEM : Scanning electron microscope
$NaBH_4$: Sodiumborohydride
k_{app} : Apparent rate constant
LDH : Layered double hydroxide
MWCNT : Multi walled carbon nanotube
M_w : Weight average molecular weight
M_n : Number average molecular weight

References

[1] Liaw, D.J., Liaw, B.Y., Li, L.I., Sillion, B., Mercier, R., Thiria, R., Sekiguchi, H. (1998) Synthesis and characterization of new soluble polyimides from 3,3',4,4'-benzhydrol tetracarboxylic dianhydride and various diamines. *Chem. Mater*. 10, 734-739.

[2] Tong, Y., Huang, W., Luo, J., Ding, M. (1999) Synthesis and properties of aromatic polyimides derived from 2,2'3,3'-biphenyletracarboxylic dianhydride. *J. Polym. Sci. Part A Polym. Chem*. 37, 1425-1433.

[3] Tanaka, K., Kita, H., Okamoto, K., Nakamura, A., Kusubi, Y. (1989) Gas permeability and permselectivity in polyimides based on 3,3',4,4'-biphenyltetracarboxylic dianhydride. *J. Membr. Sci.* 47, 203-215.

[4] Pasahan, A., Koytepe, S., Ekinci, E. (2012) Synthesis, characterization of pyridine based polyimides and their use as glucose oxidase immobilization media. *E. Polym*. 37, 1-12.

[5] Fang, X.Z., Li, Q.X., Wang, Z., Yang, Z.H., Gao, L.X., Ding, M.X. (2004) Synthesis and properties of novel polyimides derived from 2,2',3,3'-benzophenone tetracarboxylic dianhydride. *J. Polym. Sci. Part A Polym. Chem*. 42, 2130-2144.

[6] Marek, M., Schneider, B., Hlavata, D., Labsky, J., Bleha, M. (1996) Study on polyimides prepared from 3,3',4,4'-benzophenone tetracarboxylic dianhydride and 4,4'-(alkene-1-n-diyldioxy) dianilines. *J. Macromol. Sci. Pure Appl. Chem*. 33, 477-489.

[7] Lazareva, Y.N., Vidyakin, M.N., Alentiev, A.Y., Yablokova, M.Y., Kuznetsov, A.A., Ronova, I.A. (2009) Transport propertie of polyimides derived from benzophenone tetracarboxylic dianhydride and other diamines. *Polym. Sci. Ser. A,* 51, 1068-1074.

[8] Lakouraj, M.M., Rahpaima, G., Azimi, R. (2016) Organosoluble xanthone based polyimides: Synthesis, characterization antioxidant activity and heavy metal sorption. *Mater. Technol*. 50, 471-478.

[9] Yegorov, A.S., Wozniak, A.I., Ivanov, V.S., Averina, E.A., Zhdanovich, O.A. (2016) Development and optimization of producing 3,3',4,4'-benzophenone tetracarboxylic dianhydride. *Orient. J. Chem*. 32, 3063-3070.

[10] Mundhenke, R.F., Schwartz, W.T. (1990) Chemical properties of 4,4'-oxydiphthalic anhydride based polyimides. *High Peform. Polym*. 2, 57-66.

[11] Ozturk, R.D.T., Apohan, N.K., Guogor, A. (2013) Synthesis and characterization of novel polyimides based on 2,6-bis(m-aminophenoxy) benzoyl naphthalene. *Chem. Eng. Trans.* 32,1681-1686.

[12] Tanaka, K., Kita, H., Okano, M., Ikamoto, K.I. (1992) Permeability and permselectivity of gases in fluorinated and non-fluorinated polyimides. *Polymer,* 33, 585-592

[13] Mutar, M.A. (2015) New flame retardant and thermally stable PIs based on pyromellitic dianhydride and 3,3',4,4'-benzophenone tetracarboxy dianhydride with diamines containing halogens and phosphorous components in the main chain: Synthesis and characterization. *Int. J. Human. Manag. Sci*. 3, 259-268.

[14] Morikawa, A., Nabeshima, S., Satoh, A., Moriyama, Y. (2013) Synthesis and characterization of PI from 4,4'-diamino diphenylether having substituents at 2,2'-position. *J. Photopolym. Sci. Technol*. 26: 367-372.

[15] Tamai, S., Kuroki, T., Shibuya, A., Yamaguchi, A. (2001) Synthesis and characterization of thermally stable semi-crystalline PI based on 3,3'oxydianiline and 3,3',4,4'-biphenyl tetracarboxylic dianhydride. *Polymer,* 42, 2373-2378.

[16] Lee, K.W., Kowelczyk, S.P., Shaw, J.M. (1990) Surface modification of PMDA-ODA PI: Surface structure-adhesion relationship. *Macromolecules,* 23, 2018-2100.

[17] Chen, B.K., Wu, T.Y., Kuo, C.W., Peng, Y.C (2013) 4,4'-oxydianiline (ODA) containing sulfonated PI/protic ionic liquid composite mem-

branes for anhydrous proton conduction. *Int. J. Hyd. Ener*. 38, 11321-11330.

[18] Lee, K.H., Jung, J.C. (1998) Synthesis and characterization of PI from 1,4-bis[4-n-(allyloxy) phenyl] PMDA and 4,4'-oxydianiline. *Polym. Bull*. 40, 407-414.

[19] Zhao, J., Hu, Q.S., Zhou, Y.X., Peng, L., Shen, Y.Z. (2018) Preparation and properties of highly organosoluble polyimides derived from 2,2'-disubstituted 4,4'-oxydianiline. High Perform. *Polym*er, 30, 456-464.

[20] Lee, C., Shul, Y., Han, H. (2002) Dielectric properties of oxydianiline based polyimide thin films according to the water uptake. *J. Polym. Sci. Part B Polym. Phys.* 40, 2190-2198.

[21] Ivanov, V.S., Yegonov, A.S., Allakhverdov, G.R., Menshikov, V.V. (2018) Synthesis and investigation of polyimide based proton exchange membranes containing polysiloxane and crown ether moiety. *Orient. J. Chem*. 34, 255-264.

[22] Olajire, A.A., Ifediora, N.F., Bello, M.D., Benson, N.U. (2018) Green synthesis of copper nanoparticles using Alchornea laxiflora leaf extract and their catalytic application for oxidative desulfurization of model oil. *Iran. J. Sci. Technol. Trans. A Sci*. 42, 1935–1946.

[23] Chao, M. (2018) Synthesis and characterization of semi-crystalline polyimides containing bridged linkages. *Int. J. Polym. Sci.* 2018: 1-8.

[24] Rimdusit, S., Benjapan, W., Assabumrungrat, S., Takeichi, T., Yokoto, R. (2007) Surface segregation of siloxane containing component in polysiloxane-block-polyimide and s-BPDA/ODA polyimide blends. *Polym. Eng. Sci.* 47: 489-498.

[25] Patel, C.B., Patel, H.S. (1999) Polyimide based on novel multifunctional maleimide derivative. *Polym. Eng. Sci*. 39, 1489 -1492.

[26] Fang, X., Yang, Z., Zhang, S., Gao, L., Ding, M. (2002) Polyimides derived from mellophanic dianhydride. *Macromolecules,* 35, 8708-8717.

[27] Wu, F., Zhou, X., Yu, X. (2017) Synthesis and characterization of novel star branched polyimidesderived from 2,2'-bis[4-(2,4-diaminohenyl] hexafluoropropane. *RSC Adv.* 7, 35786-35794.

[28] Seo, J., Lee, A., Oh, J., Han, H. (2000) Effect of diamines (1,4-phenyl-diamine and 4,4'-dianhydride) on water sorption behaviour of polyimide thin film. *Polym. J.* 32, 583-588.

[29] Huang, Y., Ma, H., Wang, S., Shen, M., Shi, X. (2012) Efficient catalytic reduction of hexavalent Chromium using Palladium nanoparticle immobilized electrospun polymer nanofibers. *Appl. Mater. Inter*. 4, 3054 -3061.

[30] Das, B., Sharma, M., Sarmah, J.C., Bania, K.K. (2017) Rapid reduction of dye pollutants and hexavalent chromium by silver-sulphur oxido-vanadium cluster. *J. Env. Chem. Eng*. 5, 4212 -4219.

[31] Pandey, N., Shukla, S.K., Singh, N.B (2017) Water purification by polymer nanocomposites: an overview. *Nanocomposites,* 3, 47-66.

[32] Lee, M., Yen, B., Den, W. (2015) Chitosan as a natural polymer for heterogeneous catalysts support: A short review on its applications. *Appl. Sci*. 5, 1272 -1283.

[33] Khan, J., Siddiqu, M., Akram, B., Ashraf, M.A. (2018) In-situ synthesis of CuO nanoparticles in Poly(NIPAM-co-AAA) microgel, structural characterization, catalytic and biological applications. *Arab. J. Chem*. 11, 897 -909.

[34] Pozun, Z.D., Keller, E., Tran, K., Tang, W., Henkelman, G. (2013) A systematic investigation of *p*-nitrophenol reduction by bimetallic dendrimer encapsulated nanoparticles. *J. Phys. Chem. C,* 117, 7598-7604.

[35] Islam, M.T., Domeniguez, N., Ahsan, M.A., Alvarez, J.J., Noveroh, J.C. (2017) Sodium rhodizonate induced formation of gold nanoparticles supported on cellulose fibers for catalytic reduction of 4-nitrophenol and organic dyes. *J. Env. Chem. Eng*. 5, 4185 -4193.

[36] Ali, I., Jamil, N. (2018) Biosynthesis and characterization of poly3-hydroxyalkonate (PHA) from newly isolated bacterium basillus sp. A2R1. *Iran. J. Sci. Technol. Trans. A Sci.* 42: 371-378.

[37] Mei, Z.Y., Wei, Z.X., Sheng, C.D., Fang, L., Tan, X., Farag, A.S. (2017) Synthesis of single-crystal hyperbranched rhodium nanoplates with remarkable catalytic properties. *Sci. Chin*. 60, 685-696.

[38] Liou, G.S., Hsiao, H.H. (2002) Synthesis and properties of new soluble aromatic polyamides and polyimides on the basis of N,N′-bis(3-aminobenzoyl)-N,N′-diphenyl-1,4-phenylenediamine. *J. Polym. Sci. Part A Polym. Chem.* 40, 2564-2574.

[39] Arbash, A., Ahmad, Z., Sagheer, A.F., Ali, A.A.M. (2006) Microstructure and thermomechanical properties of polyimide-silica nanocomposites. *J. Nanomat*. 2006, 1–9.

[40] Jwo, S.L., Whang, W.T., Liaw, W.C. (1999) Effects of the solubility parameter of polyimides and the segment length of siloxane block on the morphology and properties of poly(imide siloxane*). J. Appl. Polym. Sci.* 74, 2832-2847.

[41] Liu, Y., Jiang, G., Li, L., Chen, H., Huang, Q., Jiang, T., Du, X., Chen, W (2015) Preparation of Au/PAN nanofibrous membranes for catalytic reduction of 4-nitrophenol. *J. Mater. Sci.* 50, 8120–8127.

[42] Patnaik, S., Das, K.K., Mohanty, A., Parida, K. (2018) Enhanced photo catalytic reduction of Cr(VI) over polymer-sensitized g-C_3N_4/$ZnFe_2O_4$ and its synergism with phenol oxidation under visible light irradiation. *Catal. Today,* 315, 52-66.

[43] Saranya, G., Kaviya, M., Meenarathi, B., Anbarasan, R. (2017) Synthesis, characterization and catalytic activity of chitosan Shiff base/V_2O_5 nanocomposite. *Int. J. Chem. Biol. Sci.* 3, 18-40.

Appendices: Supporting information

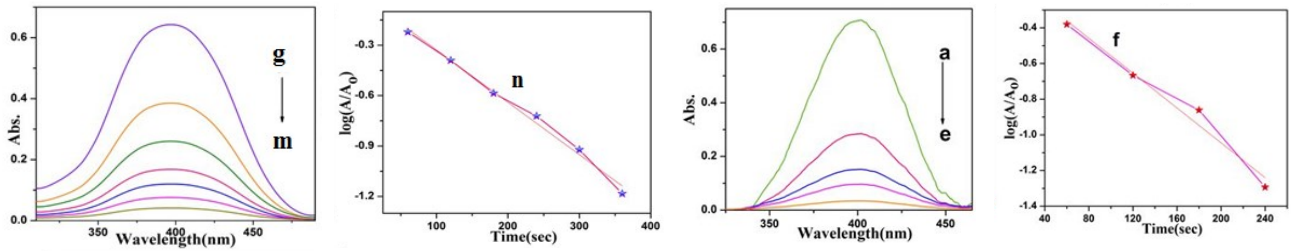

Figure A1. UV-visible spectra of (a–e) NiP, plot of time vs. log (A/A_o) (f) in the presence of P2 system, UV-visible spectra of (g–m) NiP, plot of time vs. log (A/A_o) (n) in the presence of P5 system.

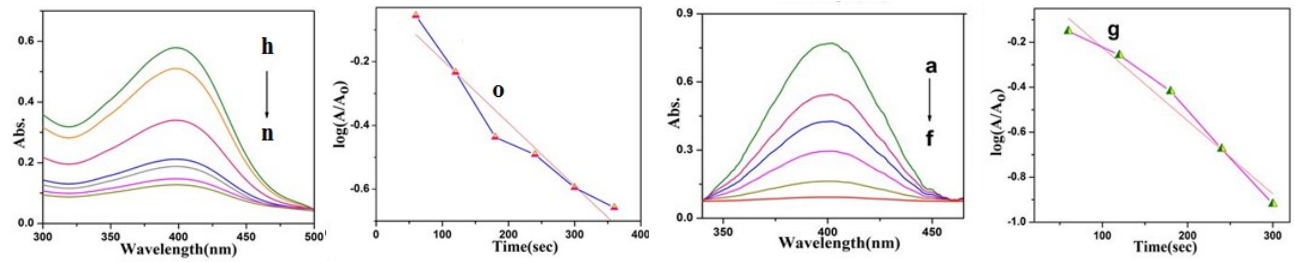

Figure A2. UV-visible spectra of (a–f) NiP, plot of time vs. log (A/A_o), (g) in the presence of P3 system, UV-visible spectra of (h–n) NiP, plot of time vs. log (A/A_o), (o) in the presence of P6 system.

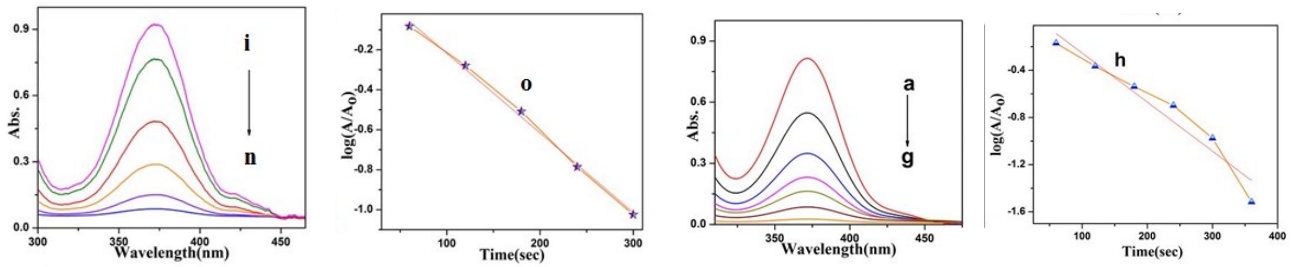

Figure A3. UV-visible spectra of (a–g) Cr(VI), plot of time vs. log(A/A_o) (h) in the presence of P2 system, UV-visible spectra of (i–n) Cr(VI), plot of time vs. log(A/A_o) (o) in the presence of P5 system.

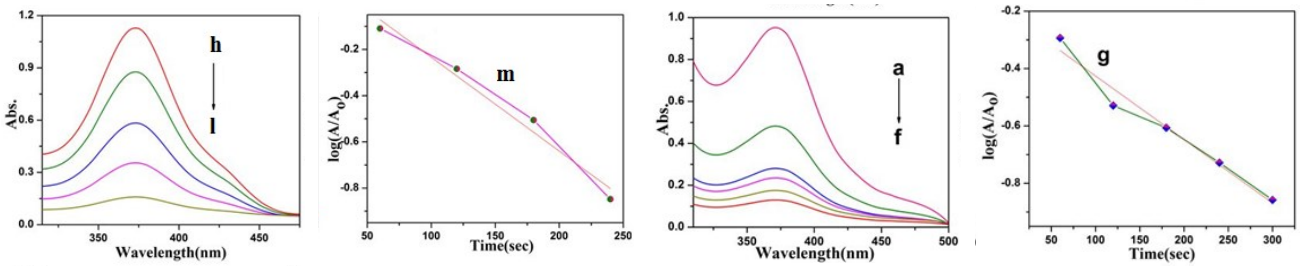

Figure A4. UV-visible spectra of (a–f) Cr(VI), plot of time vs. log (A/A_o) (g) in the presence of P3 system, UV-visible spectra of (h–l) Cr(VI), plot of time vs. log (A/A_o) (m) in the presence of P6 system.

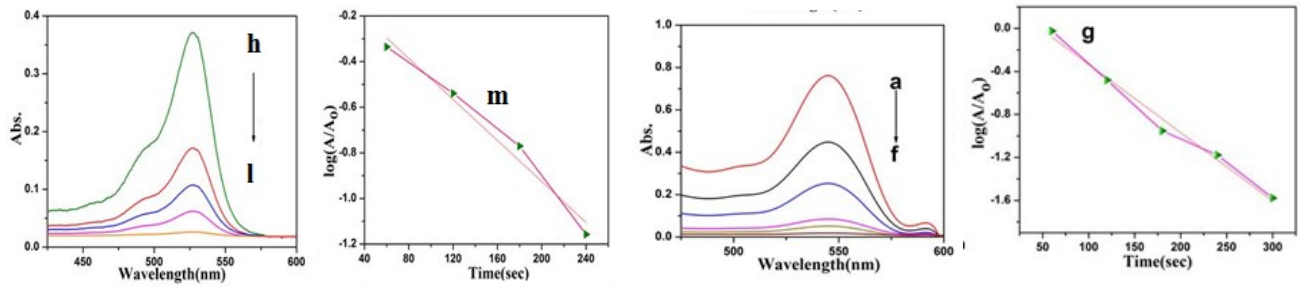

Figure A5. UV-visible spectra of (a–f) R6G, plot of time vs. log(A/A$_o$) (g) in the presence of P2 system, UV-visible spectra of (h–l) R6G, plot of time vs. log(A/A$_o$) (m) in the presence of P5 system.

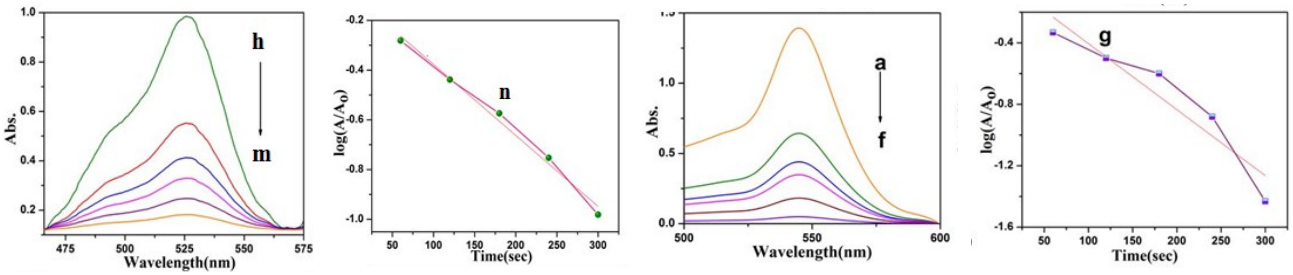

Figure A6. UV-visible spectra of (a–f) R6G, plot of time vs. log (A/A_o) (g) in the presence of P3 system, UV-visible spectra of (h–m) R6G, plot of time vs. log (A/A_o) (n) in the presence of P6 system.